JPE 17-4-13

https://doi.org/10.6113/JPE.2017.17.4.972
ISSN(Print): 1598-2092 / ISSN(Online): 2093-4718

Application of Multiple Parks Vector Approach for Detection of Multiple Faults in Induction Motors

Tushar G. Vilhekar[†], Makarand S. Ballal[*], and Hiralal M. Suryawanshi[*]

[†,*]Department of Electrical Engineering, Visvesvaraya National Institute of Technology, Nagpur, India

Abstract

The Park's vector of stator current is a popular technique for the detection of induction motor faults. While the detection of the faulty condition using the Park's vector technique is easy, the classification of different types of faults is intricate. This problem is overcome by the Multiple Park's Vector (*MPV*) approach proposed in this paper. In this technique, the characteristic fault frequency component (*CFFC*) of stator winding faults, rotor winding faults, unbalanced voltage and bearing faults are extracted from three phase stator currents. Due to constructional asymmetry, under the healthy condition these characteristic fault frequency components are unbalanced. In order to balanced them, a correction factor is added to the characteristic fault frequency components of three phase stator currents. Therefore, the Park's vector pattern under the healthy condition is circular in shape. This pattern is considered as a reference pattern under the healthy condition. According to the fault condition, the amplitude and phase of characteristic faults frequency components changes. Thus, the pattern of the Park's vector changes. By monitoring the variation in multiple Park's vector patterns, the type of fault and its severity level is identified. In the proposed technique, the diagnosis of faults is immune to the effects of unbalanced voltage and multiple faults. This technique is verified on a 7.5 *hp* three phase wound rotor induction motor (*WRIM*). The experimental analysis is verified by simulation results.

Key words: Bearing fault Park's vector (*BFPV*), Multiple Park's vector (*MPV*), Rotor fault Park's vector (*RFPV*), Stator fault Park's vector (*SFPV*), Unbalanced voltage Park's vector (*UVPV*), Wound rotor induction motor (*WRIM*)

I. INTRODUCTION

The wound rotor induction motor (*WRIM*) is a versatile induction motor. It is generally recommended for a high starting torque with a reduced inrush current. The *WRIM* is commonly used for industrial and marine applications, exhaust fan and blowers, crushers, cranes, hoists, chippers, conveyors, etc. Variations in the load, hostile environments, dirt contamination in windings and bearings, poor lubricant in the bearing, and power supply problems, can all lead to failures in the stator winding, rotor winding and bearings [1], [2]. The statistics for the commonly occurring faults in induction motors are given in Table I [2]-[4]. These faults result in reductions in efficiency, overheating, unbalanced magnetic forces, ripple in torque, vibration, etc. If these faults are not detected in the incipient stage, they may result in a catastrophic failure in the WRIM. This may result in a loss of production due to unwanted downtime, financial loss in term of the maintenance/replacement of machines and the time involved in such operations. In order to avoid this, these faults need to be detected at the incipient level.

The literature related to stator winding, rotor winding and bearing faults is given Table II. It is noticed that Cardoso et al. reported the Parks vector approach for the detection of stator winding faults [10]. It is observed that the Park's vector approach is simple and easy to analyze. However, under unbalanced voltage condition it is difficult to conclude whether the variation in stator currents Park's vector pattern is due to a stator winding fault or unbalanced voltage. Similarly, under unbalanced voltage condition the detection of bearing and rotor winding faults is difficult. If multiple faults occurs simultaneously it is difficult to detect which type of fault has occurred. In order to overcome this problem the Extended Parks vector approach was reported in [24], [26] by Cruz *et al*. This approach is able to detect and classify the type of fault. However, this approach requires an expert opinion. The Parks vector approach is easy to analyze but makes it difficult to classify multiple faults. Where, in the

Manuscript received Jan. 6, 2017; accepted Apr. 1, 2017
Recommended for publication by Associate Editor Kwang-Woon Lee.
[†]Corresponding Author: tushar.vilhekar@gmail.com
Tel: +91-8975848790, Visvesvaraya National Institute of Technology
[*]Dept. of Electrical Eng., Visvesvaraya National Institute of Tech., India

TABLE I
STATISTICS ON THE OCCURRENCE OF FAULTS IN IMS

Type of fault	IEEE-IAS % of failure	EPRI % of failure	Allianz % of failure
Stator fault	26	36	66
Rotor fault	8	9	13
Bearing fault	44	41	13
Other faults	22	14	8

TABLE II
TECHNIQUES PROPOSED FOR THE DETECTION OF VARIOUS FAULTS

Techniques	ADVANTAGES	Limitation	Ref.
Stator faults			
Magnetic pendulum oscillation	Immune to noise	Unable to detect fault location	[5]
External stray flux analysis	Economic, Immune to unbalanced voltage	Depend on sensor position	[6]
Negative sequence impedance	Not affected by construction asymmetry	Unbalanced voltage affected detection at small severity	[7], [8]
Double Park's vector	Immune to unbalanced voltage	Less sensitive low fault severity	[9]
Pattern based	Identify fault location, easy to analyzed	Unbalanced voltage affected detection	[10]-[13]
Rotor faults			
Neural network	Immune to intrinsic electric and magnetic asymmetry	Requires accurate data and rigorous training	[14]-[16]
Stator and rotor currents	Not affected by load oscillation	Requires expert opinion	[17]-[20]
Space harmonics	Low cost, Non invasive	Requires expert opinion	[21]-[23]
Extended and Park's vector	Reduced computation	Unable to detect fault location	[24]-[26]
Short Freq. Fourier transform	Reduced computational requirement	Requires expert opinion	[27]
Bearing faults			
Stator current	More accurate	Requires expert opinion	[28]-[30]
Shaft neutral voltage	Simple and easy to monitor	Types of faults difficult to classify	[31]
Shaft current	Classify single point or generalized fault	Less sensitive lower power rating	[32]
Autoregressive stator current	Immune to voltage variation	Difficult to classify types of faults	[33]
Instantaneous frequency	Not affected by noise	Requires expert opinion	[34]
Proposed technique	Immune to unbalanced voltage, detect multiple fault and its severity	Not reported in literature	

case of Extended Parks vector approach, it is easy to classify the type of faults but difficult to analyzed it. By combining the advantages of both of these approaches (*i.e.* Parks vector and Extended Parks vector) a novel Multiple Park's Vector (*MPV*) approach is proposed in this paper. The advantages of the proposed technique make it easy to analyze faults. This technique is able to classify multiple faults, immune to unbalance supply voltage. In addition, it is a non-invasive technique that can detect the fault severity. Furthermore, in the case of winding faults the proposed technique can identify the winding fault location (*i.e.* phase in which fault occurred). In the case of a winding fault, the proposed technique can identify the winding fault location (*i.e.* phase in which winding fault occurred). It also gives information about unbalance in the phase voltages.

In the present technique, a *FFT* (fast Fourier transform) of the stator currents is analyzed for stator faults, rotor faults, unbalanced voltage and bearing faults. The characteristic fault frequency components (*CFFC*) for each of the faults are extracted. Under the healthy condition, due to constructional asymmetry, the *CFFC* of particular fault are unbalanced in terms of the amplitude and phase. Under such condition, the Park's vector patterns of the *CFFC* is not circular in shape. In order to have the Park's vector pattern circular under the healthy condition, a correction factor is added in the *CFFC* of each phase stator current. By monitoring the variation in the *MPV* patterns, the type of faults and their severity is identified.

II. ANALYTICAL APPROACH

The winding representation of the stator and rotor winding for an *a* phase winding fault in the stator winding and rotor winding is shown in Fig. 1, where, sa_2 and ra_2 represent stator and rotor faulty windings for α (no of turns shorted in the stator winding/total number of turns per phase in the stator winding) and β (no of turns shorted in the rotor winding/total number of turns per phase in the rotor winding) fraction of turns shorted, respectively. For the healthy condition, α and β are zero. The mathematical expression for the stator voltage in term of the flux linkage and current is [35]:

$$[v_s] = [R_s][i_s] + \rho[\lambda_s] \tag{1}$$

Where:

$$\begin{aligned} [v_s] &= \begin{bmatrix} v_{sa1} & v_{sa2} & v_{sb} & v_{sc} \end{bmatrix}^T, \\ [i_s] &= \begin{bmatrix} i_{sa} & (i_{sa} - i_f) & i_{sb} & i_{sc} \end{bmatrix}^T, \\ R_s &= R_s \; diag \; \begin{bmatrix} 1-\alpha & \alpha & 1 & 1 \end{bmatrix}, \\ \lambda_s &= L_{ss} i_s + L_{sr} i_r \end{aligned} \tag{2}$$

the suffixes *s* and *r* denote the parameters associated with the stator winding and rotor winding, respectively. The parameters *R* and *L* denote the resistance and inductance of

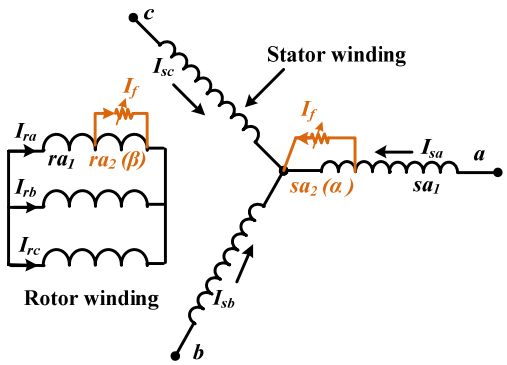

Fig. 1. Schematic diagram of the stator winding and rotor winding for stator winding and rotor winding faults.

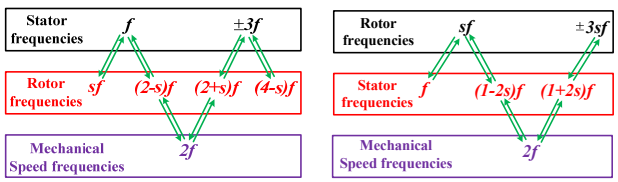

(a) Stator winding fault. (*b*) Rotor winding fault.

Fig. 2. Frequency propagation.

the winding. The parameters *v*, *i* and λ represents the voltage, current and flux linkage, respectively. L_{ls} and L_{ms} indicate the leakage and magnetizing inductance of the winding, respectively. The self and mutual inductances are given in the appendix. From Equ. (1), the stator currents is expressed as below:

$$[i_s]=[R_s]^{-1}\{[v_s]-\rho[\lambda_s]\} \tag{3}$$

A. Relationship between Stator Winding Faults and the Stator Current

From Equ. (3), it is observed that the current in the stator winding depends on the stator winding resistance and flux linkage. The flux linkage of the stator winding depends on the self-inductance of the stator winding and the mutual inductance with the rotor winding Equ. (2). which is as expressed below [36]:

$$L_{ss}=\frac{\mu_0 \Re \pi l N_s^2}{2g} \tag{4}$$

$$L_{sr}=\frac{\mu_0 \Re \pi l N_s N_r}{4g} \tag{5}$$

Where, μ_0 and $\Re$ represents the permeability of air and the mean radius of the air-gap, respectively. *l* and *g* denote the length of the rotor and the air-gap, respectively. From Eqns. (4) and (5) it is observed that the self and mutual inductances of the stator winding are proportional to the number of turns in the stator winding (N_s). Therefore, from Eqns. (2)-(5), the stator current is a function of the number of turns in the stator winding.

$$i_s=f_1(N_s) \tag{6}$$

The *WRIM* frequency propagation of a stator winding fault is shown in Fig. 2(a). It is noticed that the 3rd order harmonic component represents the *CFFC* for a stator winding fault (due to stator winding asymmetry) [37]. Hence, during the stator winding fault condition, the 3rd order harmonic component is produced in the stator currents.

B. Relationship between Rotor Winding Faults and the Stator Current

The stator current depends on the mutual inductance between the stator winding and the rotor winding from Eqns. (2)-(3). The mutual inductance between the stator winding and the rotor winding is proportional to the number of turns in the rotor winding (N_r), as expressed in Equ. (5). Therefore, from Eqns. (2), (3) and (5) the stator current is a function of the number of turns in the rotor winding.

$$i_s=f_2(N_r) \tag{7}$$

The *WRIM* frequency propagation of a rotor winding fault is shown in Fig. 2(b). The 3rd order harmonic component of the slip frequency in the rotor current represents the *CFFC* for a rotor winding fault (due to rotor winding asymmetry), which is reflected as the (1±2*s*) order *CFFC* in the stator currents. Therefore, the (1±2*s*) order harmonic component represents the *CFFC* for a rotor winding fault in the stator currents [37].

C. Relationship between Unbalanced Voltage and the Stator Current

From Equ. (3), the stator current depends on the supply voltage. Therefore, the stator current is a function of the supply voltage.

$$i_s=f_3(v_s) \tag{8}$$

An unbalance in the supply voltage produces negative sequence component which, produces the 2nd order *CFFC* in the stator currents. Hence, the 2nd order represents the *CFFC* for an unbalanced voltage.

D. Relationship between Bearing Faults and the Stator Current

The electromagnetic torque in term of electrical quantities is expressed as [36]:

$$T_{em}=i_s\frac{\partial}{\partial\theta_r}L_{sr}i_r \tag{9}$$

The dynamic electromagnetic torque in terms of the rotor speed and damping coefficient is expressed below [38]:

$$T_{em}=T_m+J\rho\omega+B\omega \tag{10}$$

Where, θ_r, T_m, and *J* represents the rotor angular position, mechanical torque and moment of inertia of a rotor connected to a load, respectively. *B* and ω denote the damping coefficient and instantaneous angular speed of the *WRIM*, respectively. The term $J\rho\omega$ represents dynamic torque under the transient condition. From Eqns. (9)-(10), the stator current

in term of the damping coefficient is expressed as below:

$$i_s = (T_m + J\rho\omega + B\omega) / (\frac{\partial}{\partial \theta_r} L_{sr} i_r) \quad (11)$$

A failure in the bearings leads to an increase in the friction of the *WRIM* [38], which is further reflected in terms of the damping coefficient. Under the bearing failure condition the damping coefficient is increased. In order to supply the load demand, the stator current has to be increased. This means that the stator current is a function of the bearing failure *i.e.* the damping coefficient.

$$i_s = f_4(B) \quad (12)$$

Basically, there are four types of bearing faults *i.e.* ball faults, cage damage, and inner and outer raceway bearing faults. To verify the proposed technique, an outer raceway fault is considered (pit). The *CFFC* for outer raceway faults is expressed as below [34]:

$$f_o = \frac{n}{2} f_m [1 - \frac{BD}{PD} \cos\gamma] \quad (13)$$

Where, n and f_m represent the number of balls in the bearing and the mechanical frequency, respectively. *BD* and *PD* denote the ball diameter and bearing pitch diameter, respectively, while γ indicates the ball contact angle.

E. Correction Factor

Under the healthy condition, the three phase stator current is balanced in terms of amplitude and phase as expressed below:

$$\begin{aligned} i_{sa} &= I_m \sin(\omega t) \\ i_{sb} &= I_m \sin(\omega t - 120^\circ) \\ i_{sc} &= I_m \sin(\omega t - 240^\circ) \end{aligned} \quad (14)$$

However, under the stator winding fault condition, the 3rd order harmonic component represents the *CFFC*. Under the healthy condition the 3rd order *CFFC* is present in the stator current due to winding asymmetry, which is expressed as below:

$$\begin{aligned} i_{sa_{sf}} &= I_{ma_{sf}} \sin 3(\omega t) \\ i_{sb_{sf}} &= I_{mb_{sf}} \sin 3(\omega t - 120^\circ) = I_{mb_{sf}} \sin 3(\omega t) \\ i_{sc_{sf}} &= I_{mc_{sf}} \sin 3(\omega t - 240^\circ) = I_{mc_{sf}} \sin 3(\omega t) \end{aligned} \quad (15)$$

From Equ. (15) it is noticed that the phase shift between the 3rd order harmonic components is not equal to 120. In addition, because of constructional asymmetry, the amplitude of the 3rd order *CFFC* for all of the phases are not the same. Therefore, under such conditions the stator fault Park's vector (*SFPV*) pattern is not circular in shape. In order to have a circular pattern, a correction factor is added to the amplitude and phase of the *CFFC* of the three phase stator currents. As a result, the amplitudes of the three phases are unity and the shift between them is 120. The 3rd order *CFFC* of the three phase stator currents after adding a correction factor is expressed as below:

$$\begin{aligned} i_{sa_{sf}} &= I_{ma_{sf}} \hat{I}_{a_{sf}} \sin(3\omega t + \phi_{a_{sf}}) \\ i_{sb_{sf}} &= I_{mb_{sf}} \hat{I}_{b_{sf}} \sin(3\omega t + \phi_{b_{sf}}) \\ i_{sc_{sf}} &= I_{mc_{sf}} \hat{I}_{c_{sf}} \sin(3\omega t + \phi_{c_{sf}}) \end{aligned} \quad (16)$$

Where, $\hat{I}_{a_{sf}}$, $\hat{I}_{b_{sf}}$ and $\hat{I}_{c_{sf}}$ are the 3rd order harmonic amplitude correction factor in the *a*, *b* and *c* phases, respectively. $\phi_{a_{sf}}$, $\phi_{b_{sf}}$ and $\phi_{c_{sf}}$ are the 3rd order harmonic phase correction factors in *a*, *b* and *c* phases, respectively. Similarly, the (1±2*s*) order harmonic component represents the *CFFC* for rotor faults. The (1±2*s*) order harmonic components for all of the stator currents after adding a correction factor are expressed as below:

$$\begin{aligned} i_{sa_{rf}} &= I_{ma_{rf}} \hat{I}_{a_{rf}} \sin((1 \pm 2s)\omega t + \phi_{a_{rf}}) \\ i_{sb_{rf}} &= I_{mb_{rf}} \hat{I}_{b_{rf}} \sin((1 \pm 2s)\omega t + \phi_{b_{rf}}) \\ i_{sc_{rf}} &= I_{mc_{rf}} \hat{I}_{c_{rf}} \sin((1 \pm 2s)\omega t + \phi_{c_{rf}}) \end{aligned} \quad (17)$$

The 2nd order harmonic component represents the *CFFC* for an unbalanced voltage. The 2nd order harmonic components of the three phase stator currents after adding a correction factor is expressed below:

$$\begin{aligned} i_{sa_{uv}} &= I_{ma_{uv}} \hat{I}_{a_{uv}} \sin(2\omega t + \phi_{a_{uv}}) \\ i_{sb_{uv}} &= I_{mb_{uv}} \hat{I}_{b_{uv}} \sin(2\omega t + \phi_{b_{uv}}) \\ i_{sc_{uv}} &= I_{mc_{uv}} \hat{I}_{c_{uv}} \sin(2\omega t + \phi_{c_{uv}}) \end{aligned} \quad (18)$$

$\frac{n}{2} f_m [1 - \frac{BD}{PD} \cos\gamma]$ represents the *CFFC* for bearing faults. The *CFFC* of the three phase stator currents after adding a correction factor are expressed as below:

$$\begin{aligned} i_{sa_{bf}} &= I_{ma_{bf}} \hat{I}_{a_{bf}} \sin(\omega t + \phi_{a_{bf}}) \\ i_{sb_{bf}} &= I_{mb_{bf}} \hat{I}_{b_{bf}} \sin(\omega t + \phi_{b_{bf}}) \\ i_{sc_{bf}} &= I_{mc_{bf}} \hat{I}_{c_{bf}} \sin(\omega t + \phi_{c_{bf}}) \end{aligned} \quad (19)$$

Where, suffixes *sf*, *rf*, *uv* and *bf* represents parameters related to stator winding faults, rotor winding faults, unbalanced voltage and bearing faults, respectively.

F. Relationship between Multiple Park's Vector, the Stator Current and the Proposed Algorithm

Two dimensional representations of the *CFFCs* of the three phase stator currents are used for the detection of stator winding faults, rotor winding faults, unbalanced voltage and bearing faults in the *WRIM*. The Park's vector transformation is expressed as below [10]:

$$\begin{aligned} i_d &= \sqrt{\frac{2}{3}} i_{sa_{CFFC}} - \frac{1}{\sqrt{6}} i_{sb_{CFFC}} - \frac{1}{\sqrt{6}} i_{sc_{CFFC}} \\ i_q &= \frac{1}{\sqrt{2}} i_{sb_{CFFC}} - \frac{1}{\sqrt{2}} i_{sc_{CFFC}} \end{aligned} \quad (20)$$

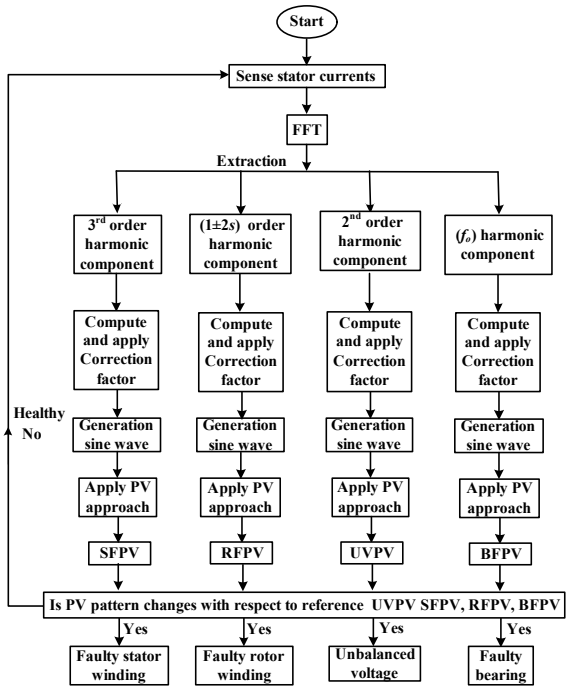

Fig. 3. Algorithm of the proposed technique.

From the above discussion, it is understood that the patterns of the Park's vector depend on the stator currents. In addition, from Eqns. (6), (7), (8) and (12), it is noticed that the stator current depends on the number of turns in the stator winding, the number of turns in the rotor winding, the supply voltage and the bearing health condition. Thus, the Park's vector pattern is a function of stator faults, rotor faults, supply voltage and bearing faults. Under healthy conditions, the Park's vector pattern is circular in shape. Whenever faults occurs in the *WRIM*, an additional frequency component is introduced in the stator currents. By continuously monitoring the Park's vector pattern of the corresponding *CFFC*, the health of the respective faults is identified. In the proposed technique, multiple faults are monitored by multiple Park's patterns. Hence, the proposed technique is referred to as Multiple Park's Vector technique (*MPV*).

The algorithm of the proposed technique is shown in Fig. 3. Where, SFPV, RFPV, UVPV and BFPV represent stator fault, rotor fault, unbalanced voltage and bearing fault Park's vectors, respectively. In the proposed technique, the CFFC for stator faults, rotor faults, bearing faults and unbalanced voltage are extracted from the three phase stator currents. The CFFC is unbalanced in amplitude and phase. Hence, to balance it, an amplitude and phase correction factor is added to it. The amplitude and phase correction factor of the CFFC is static with respect to the supply voltage and load condition. By using balanced CFFCs for each fault condition, three phase sine waves are generated. Thereafter, the Park's vector transformation is applied to convert the three phase quantity into a two phase quantity. By comparing instantaneous Park's vector patterns with reference Park's vector patterns, the health of the stator winding, rotor winding, unbalanced voltage and bearings can be identified.

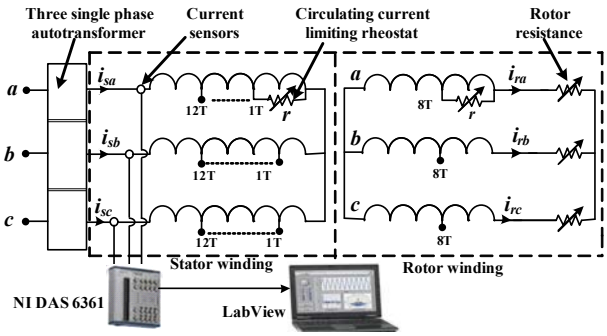

(a) Functional diagram.

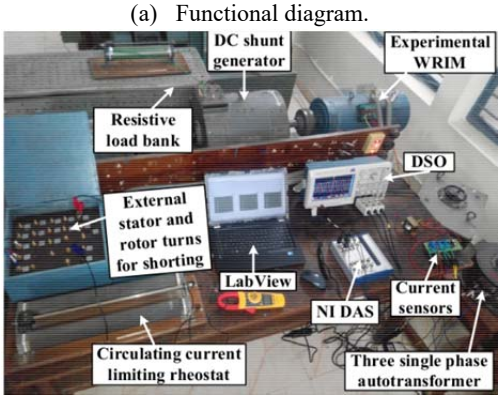

(b) Photograph of the laboratory test setup.

Fig. 4. Experimental *WRIM*.

TABLE III
DESIGN SPECIFICATION OF THE EXPERIMENTAL WRIM

Parameters	Specification
Power rating	7.5 *hp*
Stator turns/coil	57 (342 turns/phase)
Rotor turns/coil	22 (220 turns/phase)
Bearing pitch diameter (PD)	46 *mm*
Ball diameter (*BD*)	9 *mm*
Number of balls (*n*)	9
γ (assume)	0^0

III. EXPERIMENTAL SETUP

The proposed technique is experimentally verified in the laboratory on a 4 pole, 400 V, 50 *Hz WRIM*. The detailed design specifications of the experimental *WRIM* are given in Table III. A functional diagram of the experimental setup and a laboratory test setup photograph of the *WRIM* are shown in Fig. 4(a) and Fig. 4(b), respectively. In order to have a stator winding fault, seven different tappings from the stator each phase winding are taken out externally. As a result, the fault severity level can be varied from 1 turn to 12 turns shorted. Similarly, in order to have a rotor winding fault, one tap of 8 turns from each of the rotor phase winding is taken out externally through extra sliprings. The winding faults are

performed externally on the *WRIM* by connecting an external rheostat of 0-50 Ω, 20 *A* to limit the circulating current *i.e.* to control the fault severity [38]. A *FAG* make 6206 bearing is used to support the rotor of the *WRIM.* The specifications of the bearing are given in Table III. To analyze a bearing outer race fault, the bearing is damaged by drilling into the outer race. In order to load the *WRIM*, a *DC* shunt generator is coupled to the experimental *WRIM*, which is further connected to a variable resistive load bank. A Tektronix *DSO* (*DPO* 3054) is used to monitor the experimental results. *LEM* make *LA-55P* current sensors are used to sense the stator currents. The proposed algorithm is implemented in LabView® software using a NI USB 6361 data acquisition system.

IV. Experimental Results

An analysis has been carried out in four parts, *i.e.* in the first part a stator fault, in second part a rotor fault, in third part unbalance voltage and last part bearing faults are analyzed. In this analysis, the *CFFC* for stator fault, rotor fault, unbalanced voltage and bearing faults are extracted from the stator currents. To have circular Park's vector patterns, a correction factor is added in the *CFFC*. By continuously monitoring the reference *SFPV*, *RFPV*, *UVPV* and *BFPV* and the corresponding instantaneous Park's vectors, the health of the stator winding, rotor winding, unbalanced voltage and bearing are monitored. The experimental results are validated with simulation results.

A. Stator Winding Fault Analysis

The stator winding fault is one of the most commonly occurring faults in induction motors [4]. The three phase stator current FFT spectrums under healthy and 12 turns shorted in the stator a phase winding are shown in Fig. 5(a), Fig. 5(b) and Fig. 5(c). It is noticed that, the 3rd order frequency component shows a significant variation. This means that the 3rd order frequency component represents the *CFFC* for stator faults. However, the variation of the 3rd order frequency component in the *a* phase stator current is greater when compared to the other phases. This confirms that a stator winding fault has occurred in the stator *a* phase winding. A 3rd order frequency component phasor diagram of three phase stator currents under the healthy condition is shown in Fig. 5(d). In this figure, the dotted line represent the healthy condition without a correction factor, and the continuous line represents with a correction factor. This shows that the 3rd order frequency component is unbalanced in amplitude and phase. Therefore, under such conditions, the *SFPV* pattern is not circular in shape. In order to get a circular *SFPV* pattern, amplitude and phase correction is added in it. The amplitude and phase correction factor for the 3rd order *CFFC* of three phase stator currents are given in Table IV. The phasor diagram after adding correction is

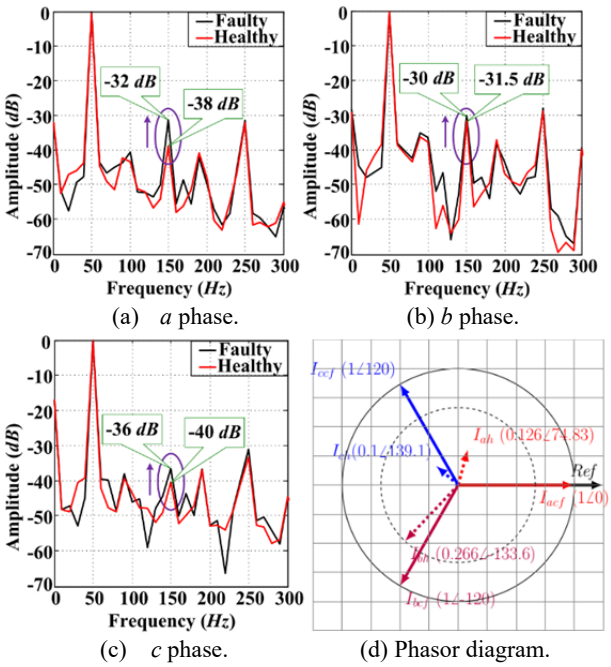

Fig. 5. Experimental stator current FFT spectrum under the healthy condition and 12 turns shorted in the stator *a* phase winding at the rated load and voltage conditions and (d) a phasor diagram of the 3rd order CFFC of the three phase stator currents under the healthy condition with and without a correction factor.

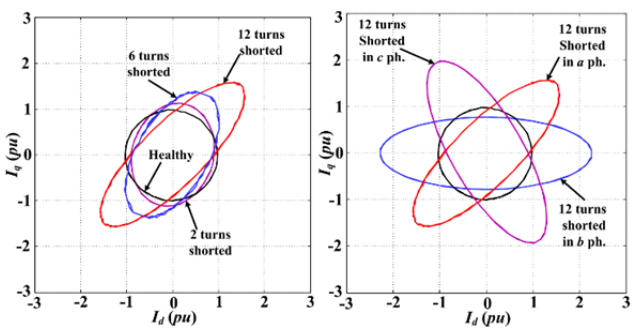

Fig. 6. Experimental SFPV patterns of the three phase stator current 3rd order frequency components under: (a) healthy and 2, 6, 12 turns shorted in the stator *a* phase winding; (b) healthy and 12 turns shorted in each phase of the stator winding at the rated load and voltage conditions.

shown in Fig. 5(d). It can be observed that the three phase 3rd order frequency components are balanced in amplitude and phase. Hence, the *SFPV* pattern of the corresponding vectors is circular in shape, as shown in Fig. 6(a).

When 12 turns of the stator *a* phase winding are shorted, this leads to a change in the amplitude and phase of the three phase stator currents 3rd order *CFFC*. The *SFPV* pattern of the corresponding 3rd order *CFFC* become elliptical in shape, as shown in Fig. 6(a). The *SFPV* pattern of the 3rd order *CFFC* three phase stator currents for 2 and 6 turns shorted in the stator *a* phase winding are shown in Fig. 6(a). This

TABLE IV
AMPLITUDE AND PHASE CORRECTION FACTOR FOR THE 3RD ORDER FREQUENCY COMPONENT

$\hat{I}_{a_{sf}}$	$\phi_{a_{sf}}$,	$\hat{I}_{b_{sf}}$	$\phi_{b_{sf}}$	$\hat{I}_{c_{sf}}$	$\phi_{c_{sf}}$
1/0.126 =7.937	-74.83	1/0.266 =3.759	13.6	1/0.1 =10	-19.1

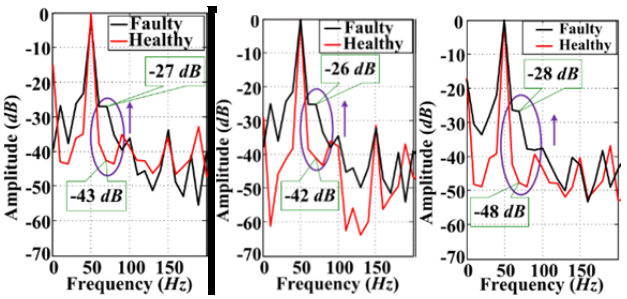

(a) *a* phase. (b) *b* phase. (c) *c* phase.

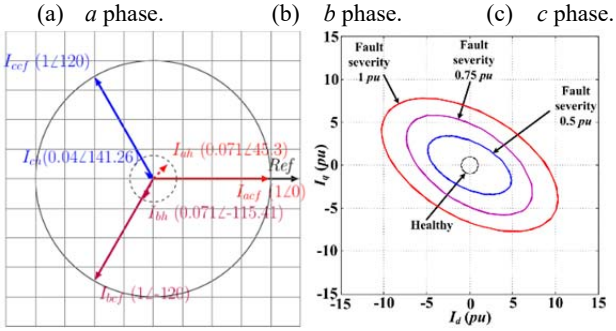

(d) Phasor diagram. (e) RFPV patterns.

Fig. 7. Experimental stator current FFT spectrum under the healthy condition and 8 turns shorted in the rotor *a* phase winding at the rated load and voltage conditions: (d) phasor diagram of the (1+2s) order CFFC of the three phase stator currents under the healthy condition with and without a correction factor at s=0.2 and (e) RFPV patterns for 8 turns shorted in the rotor *a* phase winding at 1 *pu*, 0.75 *pu* and 0.5 *pu* fault severities under the rated load and voltage conditions.

reveals that as the stator winding fault severity level increases, the amplitude of the major axis of the *SFPV* is increased and the amplitude of the minor axis of the *SFPV* is decreased. Thus, the difference between major and minor axis of the *SFPV* represents the stator winding fault severity. The *SFPV* pattern for 12 turns shorted in each of the phase stator windings are shown in Fig. 6(b). It is noticed that the orientation of the *SFPV* pattern for a stator winding fault in each phase is different. Thus, the orientation of the SFPV pattern represents the stator winding fault location (*i.e.* faulty phase).

B. Rotor Winding Fault Analysis

The rotor winding fault is one of the most commonly occurring faults in induction motors [4]. The three phase stator current *FFT* spectrum under the healthy condition and 8 turns shorted in the rotor *a* phase winding are shown in Fig. 7(a), Fig. 7(b) and Fig. 7(c). It is noticed that the (1±2s) order frequency component shows a significant variation. This means that the (1±2s) order frequency component represents the CFFC for rotor faults. However, the variations of the (1+2s) order frequency component of the stator currents in all of the phases are almost same. This is due to the fact that the air-gap stator and rotor windings are not tightly coupled. A (1±2*s*) order *CFFC* phasor diagram of the three phase stator currents under the healthy condition is shown in Fig. 7(d). It reveals that the (1±2*s*) order frequency component is unbalanced in amplitude and phase. Therefore, the *RFPV* pattern is not circular in shape. In order to get a circular *RFPV* pattern, an amplitude and phase correction factor needs to be added. The amplitude and phase correction factors for the (1+2*s*) order *CFFC* of each of the phase stator currents are given in Table V. The phasor diagram after adding a correction factor is shown in Fig. 7(d). It can be observed that the three phase (1±2*s*) order *CFFC* is balanced in amplitude and phase. Hence, the *RFPV* pattern of the corresponding vectors is circular in shape, as shown in Fig. 7(e).

TABLE V
AMPLITUDE AND PHASE CORRECTION FACTOR FOR THE (1+2S) ORDER FREQUENCY COMPONENT AT S=0.2

$\hat{I}_{a_{rf}}$	$\phi_{a_{rf}}$,	$\hat{I}_{b_{rf}}$	$\phi_{b_{rf}}$	$\hat{I}_{c_{rf}}$	$\phi_{c_{rf}}$
1/0.071 =14.09	-43.3	1/0.079 =12.66	-3.59	1/0.04 =25	-21.29

8 turns of the rotor *a* phase winding are shorted, which leads to changes in the amplitude and phase of the three phase stator currents (1±2*s*) order *CFFC*. The *RFPV* of the corresponding (1±2*s*) order *CFFC* becomes elliptical in shape, as shown in Fig. 7(e). The winding fault severity level is varied by varying the winding fault resistance, which further controls the fault circulating current, which controls the fault severity level. The *RFPV* of the (1+2*s*) order *CFFC* three phase stator currents for 8 turns shorted in the rotor *a* phase winding at 1 *pu*, 0.75 *pu* and 0.5 *pu* fault severity levels, are shown in Fig. 7(e). This reveals that when the rotor winding fault severity level decreases, the size of the *RFPV* is decreased. Thus, the size of the *RFPV* represents the rotor winding fault severity level. The RFPV is also analyzed for winding faults in the *b* phase and *c* phase rotor windings. However, the similar results are noticed as those of a winding fault in the rotor *a* phase.

C. Unbalanced Voltage Analysis

The unbalanced voltage in power systems is a common problem at the distribution level. The three phase stator current *FFT* spectrum under the healthy condition and 3% unbalanced voltage are shown in Fig. 8(a), Fig. 8(b) and Fig. 8(c). It is noticed that, the 2nd order frequency component shows a significant variation. This means that the 2nd order frequency component represents the *CFFC* for unbalanced voltage. However, the variation of the 2nd order frequency

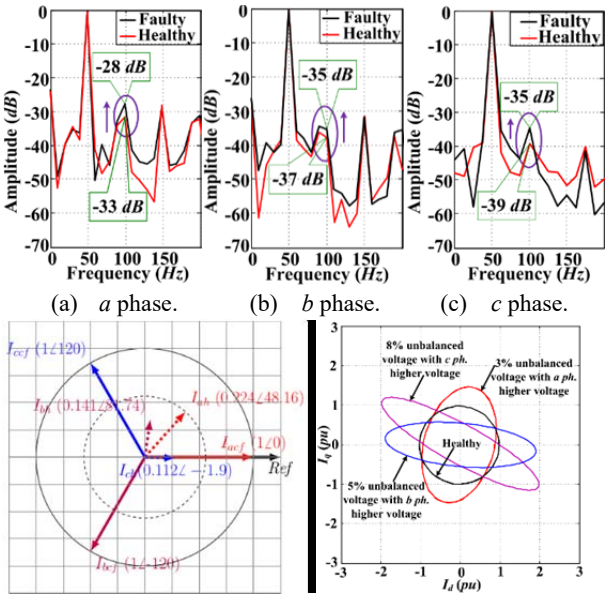

(a) *a* phase. (b) *b* phase. (c) *c* phase.

(d) Phasor diagram. (e) UVPV patterns.

Fig. 8. Experimental stator current FFT spectrum under the healthy condition and a 3% unbalanced voltage at the rated load conditions: (d) phasor diagram of the 2nd order CFFC of the three phase stator currents under the healthy condition with and without a correction factor and (e) UVPV patterns of the 2nd order CFFC three phase stator current under the healthy condition and 3%, 5% and 8% unbalanced voltages.

component of the stator *a* phase current is greater when compared to the others. As a result, the voltage amplitude of the stator *a* phase is greater when compared to the other phases. A 2nd order *CFFC* phasor diagram of the three phase stator currents under the healthy condition is shown in Fig. 8(d). This reveals that the 2nd order *CFFC* is unbalanced in amplitude and phase. Therefore, the *UVPV* pattern is not circular in shape. In order to get a circular *UVPV* pattern, a amplitude and phase correction factor needs to be added. The amplitude and phase correction factor for the 2nd order *CFFC* of the three phase stator current is given in Table VI. A phasor diagram after adding the correction factor is shown in Fig. 8(d). It can be seen that the three phase 2nd order frequency components are balanced in amplitude and phase. Hence, the *UVPV* pattern of the corresponding vectors is circular in shape, as shown in Fig. 8(e).

Under the unbalanced voltage condition, the amplitude and phase of the three phase stator current 2nd order *CFFC* changes. Therefore, the *UVPV* pattern of the corresponding 2nd order *CFFC* become elliptical in shape, as shown in Fig. 8(e). The *UVPV* for a 3% unbalanced voltage at a higher *a* phase voltage, a 5% unbalanced voltage at a higher *b* phase voltage, and a 8% unbalanced voltage at a higher *c* phase voltage are shown in Fig. 8(e). This shows that when the amount of unbalanced voltage increases, the amplitude of the *UVPV* major axis is increased and amplitude of the *UVPV* minor axis is decreased. Thus, the difference between the

TABLE VI

AMPLITUDE AND PHASE CORRECTION FACTOR FOR THE 2RD ORDER FREQUENCY COMPONENT

$\hat{I}_{a_{uv}}$	$\phi_{a_{uv}}$,	$\hat{I}_{b_{uv}}$	$\phi_{b_{uv}}$	$\hat{I}_{c_{uv}}$	$\phi_{c_{uv}}$
1/0.224 =4.46	-46.16	1/0.141 =7.09	38.26	1/0.112 =8.93	-118.1

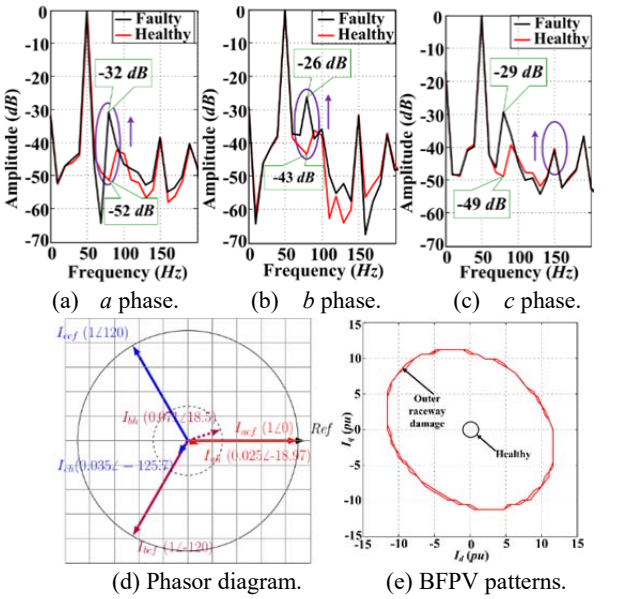

(a) *a* phase. (b) *b* phase. (c) *c* phase.

(d) Phasor diagram. (e) BFPV patterns.

Fig. 9. Experimental stator current *FFT* spectrum under the healthy condition and the outer raceway bearing damaged at the rated load conditions: (d) phasor diagram of the bearing fault *CFFC* of the three phase stator currents the under healthy condition with and without a correction factor and (e) *BFPV* patterns under the healthy condition and the outer raceway bearing damaged at the rated load and voltage conditions.

major and minor axis of the *UVPV* represents the level of the unbalance in the supply voltage. From the *UVPV* pattern it can also be seen that the orientation of the UVPV pattern for an unbalanced voltage at the *a* phase, *b* phase and *c* phase higher voltage is different. Thus, the orientation of the *UVPV* pattern represents the *a* phase, which has a higher voltage.

D. Bearing Fault Analysis

A bearing fault is the most frequently occurring fault in induction motors [4]. The three phase stator current *FFT* spectrum under the healthy condition and the bearing fault condition (outer raceway damaged) are shown in Fig. 9(a), Fig. 9(b) and Fig. 9(c). It can be noticed that the 81.45 *Hz* ($3.62x f_m$ at s=0.1) frequency component shows a significant variation. This means that the 81.45 *Hz* frequency component represents the CFFC for a bearing fault. However, a variation of the 81.45 *Hz* frequency component of the three phase stator currents are almost the same. This is due to the fact that the bearing is rotating with respect to the stator winding. A 81.45 *Hz CFFC* phasor diagram of the three phase stator currents the under healthy condition is shown in Fig. 9(d).

TABLE VII
AMPLITUDE AND PHASE CORRECTION FACTOR FOR THE BEARING FAULTS CFFC

$\hat{I}_{a_{bf}}$	$\phi_{a_{bf}}$,	$\hat{I}_{b_{bf}}$	$\phi_{b_{bf}}$	$\hat{I}_{c_{bf}}$	$\phi_{c_{bf}}$
1/0.025 =40	18.97	1/0.071 =14.085	-138.5	1/0.035 =28.571	-114.3

TABLE VIII
COMPARISON OF THE EXPERIMENTAL AND SIMULATION AREA OF THE SFPV, RFPV, UVPV AND BFPV UNDER THE RATED LOAD AND NO LOAD CONDITIONS

Types of faults	Severity of fault	Rated load		No load	
		Expt.	Simu.	Expt.	Simu.
		Area (A^2)	Area (A^2)	Area (A^2)	Area (A^2)
	Healthy	3.14	3.14	3.14	3.14
Stator	2T	3.302	3.353	3.399	3.483
	4T	3.432	3.566	3.489	3.826
	6T	3.541	3.779	3.682	4.169
	8T	3.874	3.992	3.947	4.512
	10T	4.082	4.205	4.123	4.855
	12T	4.315	4.423	5.199	4.396
Rotor 8T shorted	0.5 PU	43.895	45.207	44.89	46.128
	0.75 PU	114.14	116.423	118.7	120.28
	1 PU	222.57	224.78	229.2	231.59
Unbalanced Voltage	3%	4.351	4.437	4.524	4.573
	5%	3.13	3.193	3.236	3.439
	8%	3.424	3.842	3.475	3.42
Bearing	Outer raceway	402.32	404.24	409.3	407.65

This reveals that the 81.45 *Hz CFFC* is unbalanced in amplitude and phase. Therefore, the *BFPV* pattern is not circular in shape. In order to get a circular *BFPV* pattern, a amplitude and phase correction factor needs to be added. The amplitude and phase correction factor for a 81.45 *Hz CFFC* of the three phase stator current is given in Table VII. A phasor diagram after adding a correction factor is shown in Fig. 9(d). It can be observed that the three phase 81.45 *Hz* frequency components are balanced in amplitude and phase. Hence, the *BFPV* pattern of the corresponding vectors is circular in shape, as shown in Fig. 9(e). Under the faulty bearing condition, the amplitude and phase of the three phase stator current 81.45 *Hz CFFC* changes. Therefore, the *BFPV* pattern of the corresponding 81.45 *Hz CFFC* becomes elliptical in shape, as shown in Fig. 9(e).

E. Comparison of Experimental and Simulation Results

Experimental and simulation results of the *SFPV, RFPV*, *UVPV* and *BFPV* area under the rated load and no load conditions are given in Table VIII. The proposed experimental system is analyzed in MATLAB®. It can be observed that since the severity of the stator winding and rotor winding faults increase, the area of *SFPV* and *RFPV* are increased. In case of unbalanced voltage, when percentage of the unbalance increases, the area of the *UVPV* is decreased. From this, it can be concluded that the severity of a fault does not always depend on the area of the Park's vector. It depends on the difference between the major and minor axis. From this comparison, it can also be noticed that when the load *WRIM* increases, the area of *SFPV, RFPV, UVPV* and *BFPV* decrease. Therefore, the severity of the faults is decreased when the load on the *WRIM* increases. This is due to the fact that when the load on the *WRIM* increases, only the amplitude of the positive sequence increases when the amplitude of the negative sequence is constant. Hence, the difference between the positive and negative components is comparatively decreased. Thus, the severity of the faults decreased. The trend of the experimental results nearly matches the trend of the simulation results. Therefore, the proposed technique is verified by simulation results.

V. CONCLUSIONS

This paper introduced a new on-line and non-invasive approach for the detection of stator winding faults, rotor winding faults, unbalanced voltage and bearing faults. The *SFPV, RFPV*, *UVPV* and *BFPV* have been analyzed experimentally and simulated under healthy and faulty operating conditions. The instantaneous *SFPV, RFPV, UVPV* and *BFPV* are compared with the reference *SFPV, RFPV, UVPV* and *BFPV*. Based on the amount of deviation, the severity level of the fault is identified. Based on the orientation of the *SFPV*, the stator winding fault location is

APPENDIX

$$\mathbf{L_{ss}} = L_{ls}\begin{bmatrix}(1-\alpha) & 0 & 0 & 0\\ 0 & \alpha & 0 & 0\\ 0 & 0 & 1 & 0\\ 0 & 0 & 0 & 1\end{bmatrix} + L_{ms}\begin{bmatrix}(1-\alpha)^2 & \alpha(1-\alpha) & -(1-\alpha)/2 & -(1-\alpha)/2\\ \alpha(1-\alpha) & \alpha^2 & -\alpha/2 & -\alpha/2\\ -(1-\alpha)/2 & -\alpha/2 & 1 & -1/2\\ -(1-\alpha)/2 & -\alpha/2 & -1/2 & 1\end{bmatrix}$$

$$\mathbf{L_{sr}} = L_{sr}\begin{bmatrix}(1-\alpha)\cos\theta_r & (1-\alpha)\cos(\theta_r+2\pi/3) & (1-\alpha)\cos(\theta_r-2\pi/3)\\ \alpha\cos\theta_r & \alpha\cos(\theta_r+2\pi/3) & \alpha\cos(\theta_r-2\pi/3)\\ \cos(\theta_r-2\pi/3) & \cos\theta_r & \cos(\theta_r+2\pi/3)\\ \cos(\theta_r+2\pi/3) & \cos(\theta_r-2\pi/3) & \cos\theta_r\end{bmatrix}$$

identified. Experimental results are compared with simulation results and it is observed that the trend of the experimental results is nearly matching with the simulation results. Thus, the proposed technique is validated. The advantages of the proposed fault detection technique is that it is immune to unbalanced voltage and multiple faults.

REFERENCES

[1] A. H. Bonnett and G. C. Soukup, "Cause and analysis of stator and rotor failures in three-phase squirrel-cage induction motors," *IEEE Trans. Ind. Appl*., Vol. 28, No. 4, pp. 921–937, Jul./Aug. 1992.

[2] A. Siddique, G. S. Yadava, and B. Singh, "A review of stator fault monitoring techniques of induction motors," *IEEE Trans. Energy Convers*., Vol. 20, No. 1, pp. 106–114, Mar. 2005.

[3] "Report of large motor reliability survey of industrial and commercial installations, part I and II," *IEEE Trans. Ind. Appl.*, Vol. IA-21, No. 4, pp. 853–872, Jul. 1985.

[4] P. Zhang, Y. Du, T. G. Habetler, and B. Lu, "A survey of condition monitoring and protection methods for medium-voltage induction motors," *IEEE Trans. Ind. Appl.*, Vol. 47, No. 1, pp. 34–46, Jan./Feb. 2011.

[5] H. Mahmoud, A. A. E. Abdallh, N. Bianchi, S. M. El-Hakim, A. Shaltout, and L. Dupr, "An inverse approach for interturn fault detection in asynchronous machines using magnetic pendulous oscillation technique," *IEEE Trans. Ind. Appl.*, Vol. 52, No. 1, pp. 226–233, Jan./Feb. 2016.

[6] H. Henao, C. Demian, and G. A. Capolino, "A frequency-domain detection of stator winding faults in induction machines using an external flux sensor," *IEEE Trans. Ind. Appl.*, Vol. 39, No. 5, pp. 1272–1279, Sep./Oct. 2003.

[7] J. L. Kohler, J. Sottile, and F. C. Trutt, "Condition monitoring of stator windings in induction motors. I. experimental investigation of the effective negative-sequence impedance detector," *IEEE Trans. Ind. Appl.*, Vol. 38, No. 5, pp. 1447–1453, Sep./Oct. 2002.

[8] J. Yun, K. Lee, K. W. Lee, S. B. Lee, and J. Y. Yoo, "Detection and classification of stator turn faults and high-resistance electrical connections for induction machines," *IEEE Trans. Ind. Appl.*, Vol. 45, No. 2, pp. 666–675, Mar./Apr. 2009.

[9] T. G. Vilhekar, M. S. Ballal, and H. M. Suryawanshi, "Application of double park's vector approach for detection of inter-turn fault in induction motor," in *International Conference on Condition Assessment Techniques in Electrical Systems (CATCON)*, pp. 173–178, Dec. 2015.

[10] A. J. M. Cardoso, S. M. A. Cruz, and D. S. B. Fonseca, "Inter-turn stator winding fault diagnosis in three-phase induction motors, by park's vector approach," *IEEE Trans. Energy Convers*., Vol. 14, No. 3, pp. 595–598, Sep. 1999.

[11] H. Nejjari and M. E. H. Benbouzid, "Monitoring and diagnosis of induction motors electrical faults using a current park's vector pattern learning approach," *IEEE Trans. Ind. Appl.*, Vol. 36, No. 3, pp. 730–735, May/Jun. 2000.

[12] M. S. Ballal, D. M. Ballal, H. M. Suryawanshi, and M. K. Mishra, "Wing technique: A novel approach for the detection of stator winding inter-turn short circuit and open circuit faults in three phase induction motors," *Journal of Power Electronics*, Vol. 12, No. 1, pp. 208–214, Jan. 2012.

[13] M. S. Ballal, H. M. Suryawanshi, and B. N. Choudhari, "Extended wing technique approach for the detection of winding interturn faults in three phase transformers," *Journal of Power Electronics*, Vol. 15, No. 1, pp. 288–297, Jan. 2015.

[14] F. Filippetti, G. Franceschini, and C. Tassoni, "Neural networks aided on-line diagnostics of induction motor rotor faults," *IEEE Trans. Ind. Appl*., Vol. 31, No. 4, pp. 892–899, Jul. 1995.

[15] M. S. Ballal, H. M. Suryawanshi, and M. K. Mishra, "Detection of incipient faults in induction motors using FIS, ANN and ANFIS techniques," *Journal of Power Electronics*, Vol. 8, No. 2, pp. 181–191, Mar. 2008.

[16] J. B. Valencia, M. P. Sanchez, J. M. Roman, R. P. Panadero, and A. S. Bano, "Study of performance of several techniques of fault diagnosis for induction motors in steady-state with svm learning algorithms," in *2nd International Conference on Artificial Intelligence, Modelling and Simulation (AIMS)*, pp. 3–8, Nov. 2014.

[17] R. R. Schoen and T. G. Habetler, "Effects of time-varying loads on rotor fault detection in induction machines," *IEEE Trans. Ind. Appl.*, Vol. 31, No. 4, pp. 900–906, Jul. 1995.

[18] J. Faiz, M. Keravand, M. Ghasemi-Bijan, S. M. A. Cruz, and M. Bandar-Abadi, "Impacts of rotor inter-turn short circuit fault upon performance of wound rotor induction machines," *Electric Power Systems Research*, Vol. 135, pp. 48–58, Jun. 2016.

[19] R. Roshanfekr and A. Jalilian, "Analysis of rotor and stator winding inter-turn faults in WRIM using simulated mec model and experimental results," *Electric Power Systems Research*, Vol. 119, pp. 418–424, Feb. 2015.

[20] A. Sapena-Bano, J. Burriel-Valencia, M. Pineda-Sanchez, R. Puche-Panadero, and M. Riera-Guasp, "The harmonic order tracking analysis method for the fault diagnosis in induction motors under time-varying conditions," *IEEE Trans. Energy Convers.*, Vol. 32, No. 1, pp. 244–256, Mar. 2017.

[21] H. Henao, C. Martis, and G. A. Capolino, "An equivalent internal circuit of the induction machine for advanced spectral analysis," *IEEE Trans. Ind. Appl*., Vol. 40, No. 3, pp. 726–734, May/Jun. 2004.

[22] H. Henao, H. Razik, and G. A. Capolino, "Analytical approach of the stator current frequency harmonics computation for detection of induction machine rotor faults," *IEEE Trans. Ind. Appl.*, Vol. 41, No. 3, pp. 801–807, May/Jun. 2005.

[23] A. Yazidi, H. Henao, G. A. Capolino, and F. Betin, "Rotor inter-turn short circuit fault detection in wound rotor induction machines," in *XIX International Conference on Electrical Machines (ICEM)*, pp. 1–6, Sep. 2010.

[24] S. M. A. Cruz and A. J. M. Cardoso, "Rotor cage fault diagnosis in three phase induction motors by extended park's vector approach," *Electric Machines & Power Systems*, Vol. 28, No. 4, pp. 289–299, Nov. 2000.

[25] J. Burriel-Valencia, A. Sapena-Bao, M. Pineda-Sanchez, and J. Martinez-Roman, "Multilayer park's vector approach, a method for fault detection on induction motors," in *IEEE International Conference on Industrial Technology (ICIT)*, pp. 775–780, Mar. 2015.

[26] S. M. A. Cruz, "Diagnosis of the multiple induction motor faults using extended Park's vector approach,"

International Journal of Condition Monitoring and Diagnostic Engineering Management, Vol. 4, pp. 19–25, 2001.

[27] J. Burriel-Valencia, R. Puche-Panadero, J. Martinez-Roman, A. Sapena-Bano, and M. Pineda-Sanchez, "Short-frequency fourier transform for fault diagnosis of induction machines working in transient regime," *IEEE Trans. Instrum. Meas.*, Vol. 66, No. 3, pp. 432–440, Mar. 2017.

[28] W. Zhou, B. Lu, T. G. Habetler, and R. G. Harley, "Incipient bearing fault detection via motor stator current noise cancellation using wiener filter," *IEEE Trans. Ind. Appl.*, Vol. 45, No. 4, pp. 1309–1317, Jul./Aug. 2009.

[29] R. R. Schoen, T. G. Habetler, F. Kamran, and R. G. Bartfield, "Motor bearing damage detection using stator current monitoring," *IEEE Trans. Ind. Appl.*, Vol. 31, No. 6, pp. 1274–1279, Nov./Dec. 1995.

[30] B. Yazici and G. B. Kliman, "An adaptive statistical time-frequency method for detection of broken bars and bearing faults in motors using stator current," *IEEE Trans. Ind. Appl.*, Vol. 35, No. 2, pp. 442–452, Mar./Apr. 1999.

[31] J. M. Erdman, R. J. Kerkman, D. W. Schlegel, and G. L. Skibinski, "Effect of PWM inverters on ac motor bearing currents and shaft voltages," *IEEE Trans. Ind. Appl*., Vol. 32, No. 2, pp. 250–259, Mar./Apr. 1996.

[32] J. R. Stack, T. G. Habetler, and R. G. Harley, "Fault classification and fault signature production for rolling element bearings in electric machines," *IEEE Trans. Ind. Appl.*, Vol. 40, No. 3, pp. 735–739, May/Jun. 2004.

[33] T. G. Habetler, J. R. Stack, and R. G. Harley, "Bearing fault detection via autoregressive stator current modeling," *IEEE Trans. Ind. Appl*., Vol. 40, No. 3, pp. 740–747, May/Jun. 2004.

[34] F. Dalvand, A. Kalantar, and M. S. Safizadeh, "A novel bearing condition monitoring method in induction motors based on instantaneous frequency of motor voltage," *IEEE Trans. Ind. Electron*., Vol. 63, No. 1, pp. 364–376, Jan. 2016.

[35] R. M. Tallam, T. G. Habetler, and R. G. Harley, "Transient model for induction machines with stator winding turn faults," *IEEE Trans. Ind. Appl.*, Vol. 38, No. 3, pp. 632–637, May/Jun. 2002.

[36] P. Krause, *Analysis of electric machinery*, McGraw-Hill series in electrical and computer engineering, McGraw-Hill, 1986.

[37] Y. Gritli, L. Zarri, C. Rossi, F. Filippetti, G. A. Capolino, and D. Casadei, "Advanced diagnosis of electrical faults in wound-rotor induction machines," *IEEE Trans. Ind. Electron*., Vol. 60, No. 9, pp. 4012–4024, Sep. 2013.

[38] M. Ballal, Z. J. Khan, H. M. Suryawanshi, and R. L. Sonolikar, "Adaptive neural fuzzy inference system for the detection of inter-turn insulation and bearing wear faults in induction motor," *IEEE Trans. Ind. Electron*., Vol. 54, No. 1, pp. 250–258, Feb. 2007.

Tushar G. Vilhekar was born in Amaravati, India. He received his B.Tech. degree in Engineering from the Government College of Engineering, Amravati, India, in affiliation with Sant Gadge Baba Amravati University, Amravati, India, in 2010; and his M.Tech. degree in Power System Engineering from the College of Engineering, Pune (COEP), Pune, India, in affiliation with affiliated by Savitribai Phule Pune University, Pune, India, in 2012. He is presently working as a Research Scholar in the Department of Electricals Engineering, Visvesvaraya National Institute of Technology, Nagpur, India. His current research interests include the condition monitoring of rotating electrical machines and transformers.

Makarand S. Ballal was born in Nagpur, India. He received his B.E. in Electrical Engineering from Marathwada University, Aurangabad, India, in 1993; and hisHe received M.Tech. and Ph.D. in Electrical Engineering from Nagpur University, Nagpur, India, in 1997 and 2007, respectively. From 1997 to 2012, he was with Maharashtra State Electricity Transmission Company Limited, Maharashtra, India, where he worked on the commissioning, installation and testing of various HV and EHV electrical equipment and accessories. He was a Member of the Research and Develmpment Committe of Maharashtra State Electricity Transmission Company Limited. He is presently working as an Associate Professor in the Department of Electrical Engineering, Visvesvaraya National Institute of Technology, Nagpur, India. His current research interests include the condition monitoring and fault diagnosis of electrical machines.

Hiralal M. Suryawanshi was born in India, in 1963. He received his B.E. from Shivaji University, Kolhapur, India, in 1988; He received M.E. in Electrical Engineering from the Indian Institute of Science, Bangalore, India, in 1994; and his Ph.D. degree in Electrical Engineering from Nagpur University, Nagpur, India, in 1999. Since 2007, he has been an Professor in the Department of Electrical Engineering, Visvesvaraya National Institute of Technology, Nagpur, India. He is an Associate Editor of the IEEE Transactions on Industrial Electronics. His current research interests include the power electronics, drives and condition monitoring of electrical equipment.